IMMUNOLOGY

Local sympathetic innervations modulate the lung innate immune responses

Tingting Liu[1,2]*, Lu Yang[3]*, Xiangli Han[3], Xiaofan Ding[4], Jiali Li[5], Jing Yang[1,3,6,7,8]†

Local immunity of the lung needs to be under tight control. However, how efferent neural signals influence lung immunity remains incompletely understood. Here, we report the development of a modified iDISCO-based protocol, iDISCO(ace), for whole-tissue 3D assessment of neural innervations and immune reactions in intact, unsectioned lung tissues. We observed that genetic, pharmacologic, or surgical removal of local sympathetic innervations promoted LPS-elicited innate immune response in the lung. Also, sympathetic ablation enhanced IL-33–elicited type 2 innate immunity. We further show that the sympathetic neurotransmitter norepinephrine, or specific agonists of the β2-adrenergic receptor, can inhibit the LPS- or IL-33–elicited immune response in a cell-intrinsic manner. Moreover, genetic deletion of the β2-adrenergic receptor produced immunomodulatory effects similar to those observed with sympathetic ablation. Together, this study elucidates the critical function of local sympathetic innervations in negatively modulating the lung innate immune responses.

INTRODUCTION

Accumulating research evidence has begun to reveal that the nervous system can directly influence the body's immunity. The intriguing interplay between the nervous and immune systems have become an emerging theme in the in-depth knowledge of the immune regulation under physiological or disease conditions. Moreover, it has raised the exciting possibility that immunomodulation afforded by specific neural signals could represent the potential entry point for the treatment of different immunological disorders (*1*–*5*).

As a vital organ that is in direct contact with the outer environment, the lung is subjected to the continuous challenge of different air-borne pathogens such as viruses, bacteria, fungi, and parasites. Lung immunity, therefore, needs to not only be highly effective but also tightly controlled. Dysregulation of the local immune response in the lung would result in lethal infection, asthma, and other severe diseases (*6*–*8*). Extensive studies in the field have been focused on distinct types of immune cells, e.g., alveolar macrophages, subtypes of T lymphocytes, and innate lymphoid cells (ILCs), in the regulation of lung immune responses (*9*–*13*).

Local neural innervations in the lung have been studied for decades, with their essential roles in the respiration control well documented (*14*, *15*). However, the potential function of these local neural signals in modulating lung immunity has only begun to emerge. For instance, a previous report has shown that the parasympathetic signal could regulate spontaneous pneumonia after stroke (*16*). In addition, it was recently demonstrated that nociceptor sensory innervations inhibited the antibacterial immune response in the lung (*17*). Despite these research advances, how efferent neural signals would modulate the local immunity in the lung remains incompletely characterized. In particular, the specific function of local sympathetic innervations in the lung innate immunity is mostly unexplored. Notably, conventional immunohistochemistry methods have intrinsic limitations in assessing the three-dimensional (3D) distribution of neural innervations and immune cells in the lung. These technical shortcomings have hindered a better understanding of the complex interaction between local neural signals and different immune responses.

In this study, we report the development of a modified iDISCO protocol, iDISCO(ace) protocol for robust whole-tissue immunolabeling and 3D assessment of neural innervations and immune reactions in the intact, unsectioned lung tissues. We also demonstrate that genetic, pharmacologic, or surgical ablation of sympathetic innervations boost lipopolysaccharide (LPS)–elicited innate immunity in the lung. In addition, this loss of local sympathetic innervations promotes interleukin-33 (IL-33)–elicited type 2 innate immunity. We then show that the sympathetic neurotransmitter norepinephrine (NE), or specific agonists of the β2-adrenergic receptor, could intrinsically inhibit the LPS-elicited immune response in primary alveolar macrophages or the IL-33–elicited immune response in primary ILC2s (type 2 ILCs). Moreover, genetic deletion of the β2-adrenergic receptor induces immunomodulatory effects similar to those observed with sympathetic ablation. In summary, this study elucidates the critical role of local sympathetic innervations in negatively regulating the lung innate immune responses, which had been previously unappreciated. These findings of neuroimmune interactions in the lung could have important implications for in-depth knowledge of homeostasis and disease of this vital organ.

RESULTS

Whole-tissue 3D assessment of neural innervations and immune reactions in the lung

The recent development of several whole-mount, tissue-imaging methods, e.g., CLARITY (*18*), iDISCO$^+$ (*19*), CUBIC (*20*), and Ce3D (clearing-enhanced 3D) (*21*), has enabled the immunolabeling and 3D visualization of cellular structures in many tissue types. However, the unique presence and density of air-filled alveoli in the lung renders the immunolabeling and 3D imaging of intact, unsectioned lung tissues a challenge. We sought to optimize a procedure, based on

[1]Center for Life Sciences, Peking University, Beijing 100871, China. [2]Academy for Advanced Interdisciplinary Studies, Peking University, Beijing 100871, China. [3]School of Life Sciences, Peking University, Beijing 100871, China. [4]School of Medicine, Tsinghua University, Beijing 100084, China. [5]Kunming Institute of Zoology, Chinese Academy of Sciences, Kunming, Yunnan 650223, China. [6]IDG/McGovern Institute for Brain Research, Peking University, Beijing 100871, China. [7]State Key Laboratory of Membrane Biology, Peking University, Beijing 100871, China. [8]Institute of Molecular Physiology, Shenzhen Bay Laboratory, Shenzhen, Guangdong 518055, China.
*These authors contributed equally to this work.
†Corresponding author. Email: jing.yang@pku.edu.cn

the reported iDISCO$^+$ method (*19*), for the robust whole-tissue 3D assessment of neural innervations and immune reactions in the lung. Of importance, we noticed that although the methanol gradient pretreatment in iDISCO$^+$ was compatible with the immunolabeling of several neural markers such as PGP9.5 in the mouse lungs (fig. S1, A and B), it strongly interfered with the detection of specific immune cell markers, e.g., CD3, CD11b, and Siglec-F (fig. S1, A and B). Therefore, we screened for different organic solvents to replace the methanol-based steps of tissue permeabilization and decolorization in the original iDISCO$^+$ method. We found out that an acetone gradient pretreatment (see Materials and Methods) exhibited superior compatibility with all the tested antibodies (fig. S1, A and B). Moreover, this acetone pretreatment preserved the histologic integrity (fig. S1C) and overall structure (fig. S1D) of the mouse lungs and, at the same time, effectively facilitated the tissue decolorization and immunolabeling (Fig. 1A and see below). We named this 3D imaging procedure iDISCO(ace) to reflect both its iDISCO$^+$ origin but and the acetone-based improvement. iDISCO(ace) processes lung tissues in batches and takes approximately 7 to 10 days to complete. The immunolabeled, optically cleared tissues can be imaged by confocal microscopy or, alternatively, by lightsheet microscopy, as we have done in this study.

With this imaging power, we first examined the 3D distribution of neural innervations in the intact, unsectioned lungs of adult mice. We performed whole-tissue immunolabeling of anti-synaptophysin, the specific pan-neural marker. The 3D network of local neural innervations, with the vast majority of axons ensheathing along the lower respiratory tract, was revealed on the whole-tissue level with single-fiber resolution (Fig. 1, B and C, and movies S1 and S2). Clusters of synaptophysin-positive cells were observed adjacent to the airways

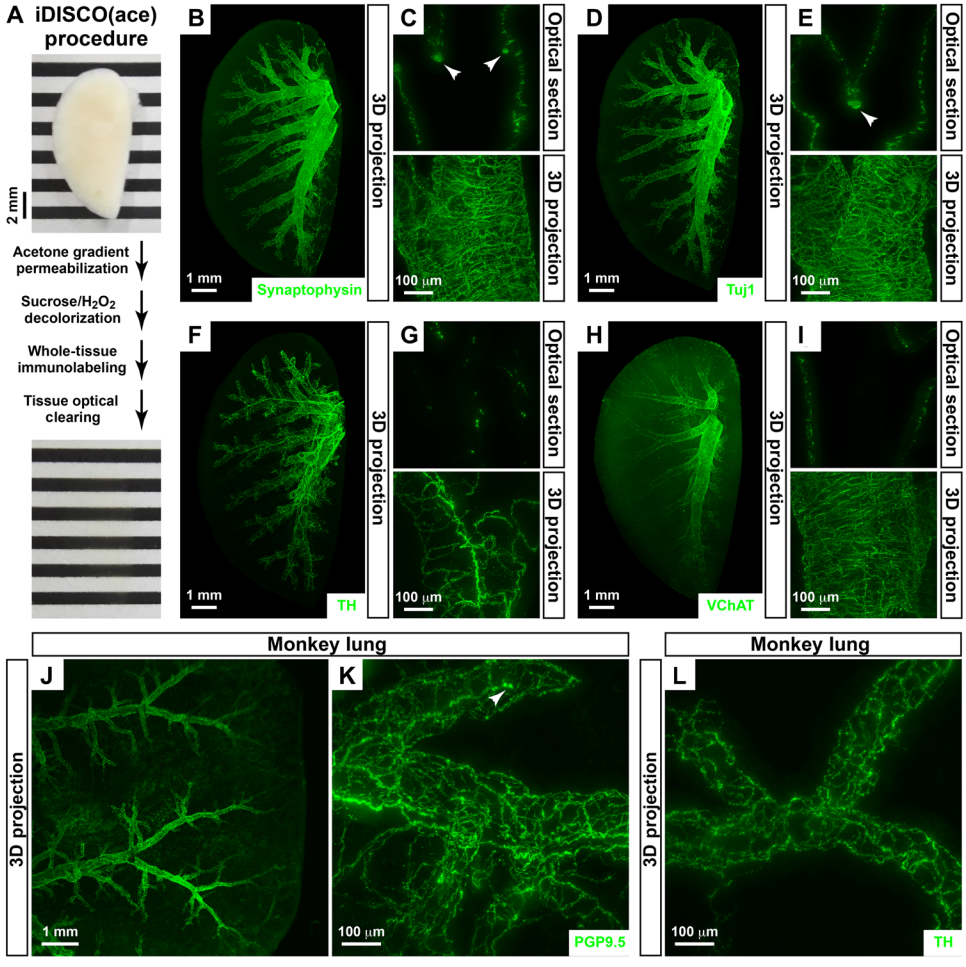

Fig. 1. Whole-tissue 3D assessment of local neural innervations in the lung tissues. (**A**) iDISCO(ace) procedure. The intact, unsectioned lung (left lobe) of the adult mouse before (top) and after (bottom) the procedure. Photo credit: Tingting Liu, Peking University. (**B** to **I**) Whole-tissue 3D assessment of local neural innervations in the mouse lung. The lungs (left lobe) of wild-type mice were processed for the whole-tissue immunolabeling of anti-synaptophysin (B and C), anti-Tuj1 (D and E), anti-TH (F and G), or anti-VChAT (H and I). (B, D, F, and H) Representative 3D projection images at ×1.26 magnification of the lightsheet imaging are shown. (C, E, G, and I) Representative optical sections (top) or 3D projection images of the 600-μm depth of the intact tissues (bottom) at ×12.6 magnification of the lightsheet imaging are shown. Arrowheads denote the clusters of neuroendocrine cells. (**J** to **L**) Whole-tissue 3D assessment of local neural innervations in the monkey lung. The lung tissues of adult macaque monkeys were processed for the whole-tissue immunolabeling of anti-PGP9.5 (J and K) or anti-TH (L). (J) Representative 3D projection images at ×1.26 magnification of the lightsheet imaging are shown. (K and L) Representative 3D projection images of the 500-μm depth of the tissues at ×12.6 magnification of the lightsheet imaging are shown. Arrowhead denotes the cluster of neuroendocrine cells.

(Fig. 1C), which represented the unique population of neuroendocrine cells in the lung (*22*, *23*). In addition, whole-tissue immunolabeling of anti-Tuj1 (neuron-specific class III β-tubulin) or anti-PGP9.5, the two additional pan-neural markers, produced a similar 3D pattern of neural innervations and neuroendocrine cell clusters (Fig. 1, D and E, and fig. S2A). Next, we performed whole-tissue immunolabeling of anti–TH (tyrosine hydroxylase), the specific sympathetic marker. The 3D network of local sympathetic innervations in the lung could be visualized (Fig. 1, F and G, and movie S3). In parallel, the whole-tissue immunolabeling of anti–VChAT (vesicular acetylcholine transporter), the specific parasympathetic marker, revealed that the density of local parasympathetic axons was about threefold higher than that of sympathetic axons (Fig. 1, H and I). Notably, iDISCO(ace) enabled effective and consistent antibody penetration through the intact mouse lungs. For instance, the whole-tissue immunolabeling of anti-synaptophysin (fig. S1, E and F) or anti-TH (fig. S1, G and H) gave rise to the uniform signal-to-background ratios across the optical sections of replicate tissue samples.

As an aside, iDISCO(ace) can also be used to process unsectioned lungs of adult macaque monkeys. The whole-tissue anti-PGP9.5 immunolabeling revealed the 3D distribution of local neural innervations, as well as the clusters of neuroendocrine cells in the monkey lung tissues (Fig. 1, J and K). In addition, local sympathetic axons ensheathing along the airways were visualized by the whole-tissue anti-TH immunolabeling (Fig. 1L).

We then applied the iDISCO(ace) procedure to imaging non-neural structures, especially cellular components related to immune reactions, in the lungs of adult mice. The whole-tissue anti-LYVE1 (lymphatic vessel endothelial receptor 1) immunolabeling exhibited the intricate lymphatic network throughout the lung (fig. S2B). In addition, we were able to examine the 3D distribution of immune cells. For instance, the wild-type mice were intranasally treated with papain or chitin, the two classic models to induce lung inflammation (*24*, *25*). The whole-tissue anti–Siglec-F immunolabeling showed the profound accumulation of Siglec-F^+ immune cells, which were predominantly eosinophils and alveolar macrophages, in both conditions (fig. S2, C and D, and movie S4). However, the 3D pattern of the immune reaction differed between the two conditions, i.e., Siglec-F^+ immune cells resided along bronchioles in the papain-treated lung but instead formed the follicle-like clusters in the chitin-treated one. Moreover, simultaneous 3D visualization of local neural innervations and immune cells could be achieved. For example, the wild-type mice were intranasally treated with LPS, a standard model of acute lung injury. The whole-tissue coimmunolabeling of anti-TH and anti-F4/80, the cellular marker for macrophage populations, revealed the spatial engagement of local sympathetic innervations with the LPS-elicited immune response (fig. S2E and see below). We noted that this intranasal LPS treatment had no detectable effect on the lymphatic network in the lungs (fig. S2B). These results together demonstrate the power of iDISCO(ace) for robust whole-tissue 3D assessment of neural innervations and immune reactions in intact lung tissues.

Local sympathetic innervations negatively modulate the LPS-elicited immune response in the lung

We focused on the potential immunomodulatory function of local sympathetic innervations in the lung, which had been mostly uncharacterized. We examined the establishment of sympathetic innervations during the mouse lung development. Sympathetic innervations were at the primary stage at postnatal day 1 (P1), as shown by the whole-tissue anti-TH immunolabeling (fig. S3A). The density of sympathetic axons increased in the lungs of P4 to P14 mice and reached the mature pattern around P21 (fig. S3A).

TrkA has been known as one of the central neurotrophin receptors in neural development (*26*). Therefore, we bred *Th-Cre; TrkA$^{fl/fl}$* mice to specifically delete the TrkA receptor in sympathetic neurons. Gross appearance of the lungs of *Th-Cre; TrkA$^{fl/fl}$* mice appeared indistinguishable from that of *Th-Cre; TrkA$^{+/+}$* control littermates (Fig. 2A). In addition, tissue weight of *Th-Cre; TrkA$^{+/+}$* and *Th-Cre; TrkA$^{fl/fl}$* lungs showed no detectable difference (Fig. 2B). However, there was a marked loss of local sympathetic innervations in *Th-Cre; TrkA$^{fl/fl}$* lungs, as revealed by the whole-tissue anti-TH immunolabeling (Fig. 2, C and D). In contrast, the whole-tissue immunolabeling of anti-VChAT (Fig. 2, E and F) or anti–CGRP (calcitonin gene-related peptide; fig. S3, B and C), the neural marker for sensory axons, exhibited no change of local parasympathetic or sensory innervations in *Th-Cre; TrkA$^{fl/fl}$* lungs, confirming the specificity of this genetic approach of sympathetic ablation. Of note, the prominent immunolabeling of CGRP-positive neuroendocrine cells was visualized along the airways (fig. S3B), consistent with a prior report that neuroendocrine cells are the major source of CGRP in the mouse lung (*27*). In addition, the anti-synaptophysin immunolabeling showed approximately 20% decrease in total axons in *Th-Cre; TrkA$^{fl/fl}$* lungs (Fig. 2, G and H), implicating that local sympathetic innervations count for about 20% of total axons. Although previous studies reported that specific types of macrophages could express TH or the TrkA receptor (*28*, *29*), the whole-tissue coimmunolabeling of anti-TH and anti-F4/80 did not reveal any TH-positive macrophages in the mouse lung (fig. S2E). In addition, we examined the expression profile of several neural markers in primary alveolar macrophages and observed the minimal gene expression of *Th* and *TrkA* (fig. S3D), suggesting that macrophages would likely not be genetically targeted in *Th-Cre; TrkA$^{fl/fl}$* lungs.

We exploited *Th-Cre; TrkA$^{fl/fl}$* mice to interrogate the immunomodulatory function of local sympathetic innervations in the lung immunity. We first examined the LPS-elicited innate immunity in the lung. The mice were intranasally treated with LPS, which resulted in the rapid recruitment of Ly-$6G^+$ neutrophils as visualized by the whole-tissue anti–Ly-6G immunolabeling (Fig. 2, I and J). The coimmunolabeling of anti–Ly-6G and anti-TH exhibited the spatial correlation between this LPS-elicited immune response with local sympathetic innervations (Fig. 2I). We then found out that the density of neutrophils was about 4×10^4 per mm^3 in LPS-treated *Th-Cre; TrkA$^{+/+}$* lungs, but it reached over 10×10^4 per mm^3 in LPS-treated *Th-Cre; TrkA$^{fl/fl}$* lungs (Fig. 2, J and K). In parallel, the fluorescence-activated cell sorting (FACS) analysis showed that $CD45^+$ $CD11b^+$ Ly-$6G^+$ neutrophils represented about 25% of $CD45^+$ cells in LPS-treated *Th-Cre; TrkA$^{+/+}$* lungs, and this percentage increased to 50% in *Th-Cre; TrkA$^{fl/fl}$* lungs (Fig. 2, L and M). Also, the FACS analysis revealed more accumulation of neutrophils in the bronchoalveolar lavage fluid (BALF) of LPS-treated *Th-Cre; TrkA$^{fl/fl}$* lungs (Fig. 2N). In addition, the histopathology of *Th-Cre; TrkA$^{fl/fl}$* lungs after the LPS treatment was more severe, as evidenced by hematoxylin and eosin (H&E) staining (Fig. 2, O and P). Moreover, this enhancement of LPS-elicited immune response resulted in the decreased survival rate of LPS-treated *Th-Cre; TrkA$^{fl/fl}$* mice compared with *Th-Cre; TrkA$^{+/+}$* littermates (Fig. 2Q). These results indicated that the genetic ablation of sympathetic innervations in the lung promoted the LPS-elicited immune response.

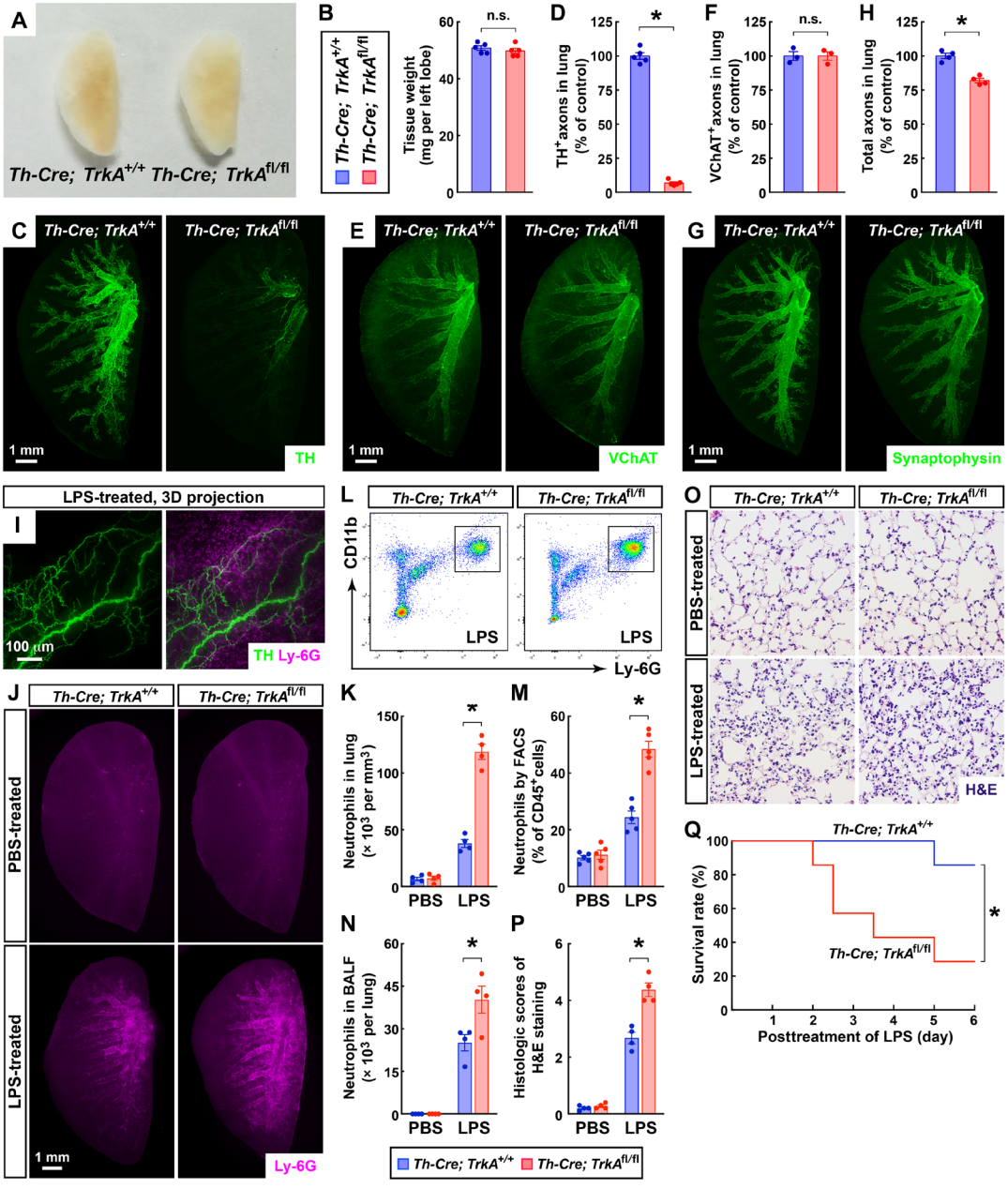

Fig. 2. Genetic ablation of local sympathetic innervations promoted the LPS-elicited innate immune response in the lung. (**A** and **B**) Normal development of the lungs of *Th-Cre; TrkA*$^{fl/fl}$ mice. (A) Gross appearance of the lungs (left lobe) of *Th-Cre; TrkA*$^{+/+}$ versus *Th-Cre; TrkA*$^{fl/fl}$ adult mice. Photo credit: Tingting Liu, Peking University. (B) The tissue weight of the lungs was quantified. $n = 5$, means ± SEM, n.s., not significant (Student's *t* test). (**C** to **H**) Genetic ablation of local sympathetic innervations in the lungs of *Th-Cre; TrkA*$^{fl/fl}$ mice. The lungs (left lobe) of *Th-Cre; TrkA*$^{+/+}$ and *Th-Cre; TrkA*$^{fl/fl}$ mice were processed for the whole-tissue immunolabeling of anti-TH (C and D), anti-VChAT (E and F), or anti-synaptophysin (G and H). (C, E, and G) Representative 3D projection images at ×1.26 magnification of the lightsheet imaging are shown. (D) TH-positive sympathetic axons were quantified. $n = 5$, means ± SEM, $^*P < 0.01$ (Student's *t* test). (F) VChAT-positive parasympathetic axons were quantified. $n = 3$, means ± SEM, n.s., not significant (Student's *t* test). (H) Synaptophysin-positive total axons were quantified. $n = 4$, means ± SEM, $^*P < 0.01$ (Student's *t* test). (**I**) Spatial engagement of local sympathetic innervations with the LPS-elicited immune response in the lung. The wild-type mice were intranasally treated with LPS. The lung (left lobe) was then processed for the whole-tissue coimmunolabeling of anti-TH (green) and anti–Ly-6G (magenta). Representative 3D projection images of the 600-μm depth of the intact tissue at ×12.6 magnification of the lightsheet imaging are shown. (**J** to **Q**) Genetic ablation of local sympathetic innervations in the lung promoted the LPS-elicited immune response. *Th-Cre; TrkA*$^{+/+}$ and *Th-Cre; TrkA*$^{fl/fl}$ mice were intranasally treated with saline control or LPS. (J and K) The lungs (left lobe) were processed for the whole-tissue anti–Ly-6G immunolabeling. (J) Representative 3D projection images at ×1.26 magnification of the lightsheet imaging are shown. (K) The density of Ly-6G$^+$ neutrophils was quantified. $n = 4$, means ± SEM, $^*P < 0.01$ (ANOVA test). (L and M) CD45$^+$ CD11b$^+$ Ly-6G$^+$ neutrophils in the lungs were examined by the FACS analysis (L) and quantified (M). $n = 5$, means ± SEM, $^*P < 0.01$ (ANOVA test). (N) CD45$^+$ CD11b$^+$ Ly-6G$^+$ neutrophils in the bronchoalveolar lavage fluid (BALF) were quantified by the FACS analysis. $n = 4$, means ± SEM, $^*P < 0.01$ (ANOVA test). (O and P) The lung tissues were assessed by H&E (hematoxylin and eosin) staining. (O) Representative images are shown. (P) The histologic scores were determined. $n = 4$, means ± SEM, $^*P < 0.01$ (ANOVA test). (Q) The survival rate of the mice was followed for 6 days after the LPS treatment. $n = 7$, $^*P < 0.05$ (log-rank test).

Because sympathetic innervations in other organs, e.g., bone marrow and spleen, were also affected in *Th-Cre; TrkA$^{fl/fl}$* mice (*30*, *31*), it became essential to validate that the sympathetic signal would regulate the lung immune response via the local mechanism. We thus devised the pharmacologic approach to ablate local sympathetic innervations in the lung specifically. The wild-type mice were intranasally treated with 6-hydroxydopamine (6-OHDA) or saline control. The gross appearance and the tissue weight of 6-OHDA–treated lungs were comparable to those of saline-treated ones (Fig. 3, A and B). However, this intranasal 6-OHDA administration effectively eliminated sympathetic axons in the lungs, as assessed by the whole-tissue anti-TH immunolabeling (Fig. 3, C and D). The anti-VChAT immunolabeling showed the normal pattern of parasympathetic innervations in 6-OHDA–treated lungs (fig. S4, A and B). There was approximately 20% loss of total axons in the 6-OHDA–treated lungs (Fig. 3, E and F), resembling that in the *Th-Cre; TrkA$^{fl/fl}$* lungs. Notably, the whole-tissue anti-TH immunolabeling of the bone marrows (inside the femurs), spleens, thymuses, and lymph nodes of 6-OHDA–treated mice exhibited no alteration of sympathetic axons in these classic immune organs (fig. S4, C to G), demonstrating the specificity of this pharmacologic ablation to local sympathetic innervations in the lungs. We then examined the LPS-elicited immune response in saline-treated and 6-OHDA–treated mice and detected stronger recruitment of neutrophils in 6-OHDA–treated lungs (Fig. 3, G and H). Also, the histopathology in response to the LPS treatment was more profound in 6-OHDA–treated lungs compared to that in the saline-treated ones (Fig. 3, I and J). In addition, similar to that observed with *Th-Cre; TrkA$^{fl/fl}$* mice, the LPS-induced mortality was significantly higher in 6-OHDA–treated mice (Fig. 3K). These results elucidated that the pharmacologic ablation of local sympathetic innervations in the lung could enhance the LPS-elicited immune response.

To further confirm the local mechanism of this sympathetic immunomodulation, we used the surgical approach of lung sympathectomy. The removal of sympathetic branches entering the pulmonary plexus led to the ablation of local sympathetic axons in the lungs, as visualized by the whole-tissue anti-TH immunolabeling (Fig. 3, L and N). As expected, this local sympathectomy did not affect sympathetic innervations in other immune organs, including the bone marrow (inside the femur), spleen, thymus, and lymph node (fig. S4, H and I). Although the local sympathectomy had the same baseline level of neutrophils in the lungs as that in the mock condition, it resulted in more neutrophil accumulation after the LPS treatment, as revealed by the anti–Ly-6G immunolabeling (Fig. 3, M and O). Together, the results obtained with the genetic, pharmacologic, and surgical approaches supported that local sympathetic innervations negatively modulate the LPS-elicited immune response in the lung.

Local sympathetic innervations suppress the IL-33–elicited type 2 innate immunity in the lung

We next explored whether local sympathetic innervations might control additional innate immune responses in the lung. The mice were intranasally treated with recombinant IL-33 protein, the common model to elicit the type 2 innate immunity. This IL-33 treatment caused the massive accumulation of Siglec-F$^+$ immune cells, as visualized by the whole-tissue anti–Siglec-F immunolabeling (Fig. 4, A and B). We noticed that these Siglec-F$^+$ immune cells showed the spatial engagement with sympathetic axons by the anti–Siglec-F and anti-TH coimmunolabeling (Fig. 4A), implicating the potential modulation of IL-33–elicited immune response by the local sympathetic signal in the lung.

Therefore, we compared *Th-Cre; TrkA$^{+/+}$* and *Th-Cre; TrkA$^{fl/fl}$* mice for the IL-33–elicited immune response. We observed a more profound accumulation of Siglec-F$^+$ immune cells in *Th-Cre; TrkA$^{fl/fl}$* lungs than that in *Th-Cre; TrkA$^{+/+}$* lungs (Fig. 4, B and C). In addition, the FACS analysis revealed that CD45$^+$ CD11c$^-$ Siglec-F$^+$ eosinophils counted for about 10% of CD45$^+$ cells in IL-33–treated *Th-Cre; TrkA$^{+/+}$* lungs, but this percentage increased to 20% in *Th-Cre; TrkA$^{fl/fl}$* lungs (Fig. 4D and fig. S5A). In addition, the histopathology after the IL-33 treatment became more severe in *Th-Cre; TrkA$^{fl/fl}$* lungs (Fig. 4, E and F). Moreover, the early up-regulation of expression levels of *IL-4*, *IL-5*, and *IL-13* in response to IL-33 was enhanced in *Th-Cre; TrkA$^{fl/fl}$* lungs (Fig. 4G), although no substantial eosinophil accumulation occurred yet. Such enhancement of type 2 cytokine expression in IL-33–treated *Th-Cre; TrkA$^{fl/fl}$* lungs could persist to a later time point (fig. S5B). We noted that no mortality occurred with the intranasal IL-33 treatment. These results suggested that the genetic ablation of sympathetic innervations in the lung boosted the IL-33–elicited innate immunity.

To support the local action of this sympathetic control of the IL-33–elicited immune response, we again exploited both the pharmacologic and surgical approaches of sympathetic ablation. We found out that the accumulation of Siglec-F$^+$ immune cells following the IL-33 treatment was significantly higher in 6-OHDA–treated lungs compared with that in saline-treated ones (Fig. 4, H and I). At the same time, 6-OHDA–treated lungs had more pronounced histopathology in response to IL-33 (Fig. 4J and fig. S5C). Furthermore, similar to that occurring with the pharmacologic ablation, the mice that underwent the lung sympathectomy exhibited stronger accumulation of Siglec-F$^+$ immune cells after the IL-33 treatment, as assessed by the whole-tissue anti–Siglec-F immunolabeling (Fig. 4, K and L). These results obtained with the three separate approaches have together demonstrated that local sympathetic innervations suppress the IL-33–elicited type 2 innate immunity in the lung.

NE cell-intrinsically inhibits the innate immune responses via the β2-adrenergic receptor signal

We set out to determine the mechanism underlying this sympathetic modulation of the lung immune responses. The sympathetic signal functions through the neurotransmitter NE. We measured the tissue content of NE and observed over 70% decrease in both *Th-Cre; TrkA$^{fl/fl}$* (Fig. 5A) and 6-OHDA–treated lungs (Fig. 5B), consistent with their drastic loss of local sympathetic innervations. Alveolar macrophages are the immune cells that can rapidly respond to the intranasal LPS challenge. We found out that the in vitro treatment of primary alveolar macrophages with NE inhibited the LPS-elicited expression of cytokines and chemokines, including *TNFα*, *CCL2*, and *CXCL2* (Fig. 5C). Notably, CXCL2 is one of the central chemokines for neutrophil recruitment during inflammation (*32*, *33*). Intravenous administration of an anti-CXCL2 neutralizing antibody was sufficient to mitigate the enhanced neutrophil recruitment in 6-OHDA–treated lungs after the LPS treatment (fig. S5, D and E). In parallel, ILC2s are known for their central role in the innate immune response to IL-33 (*34*–*37*). We showed that the in vitro NE treatment of primary ILC2s isolated from the lungs suppressed the IL-33–elicited expression of *IL-4*, *IL-5*, and *IL-13* (Fig. 5D). These results suggested that the sympathetic neurotransmitter NE could cell-intrinsically inhibit

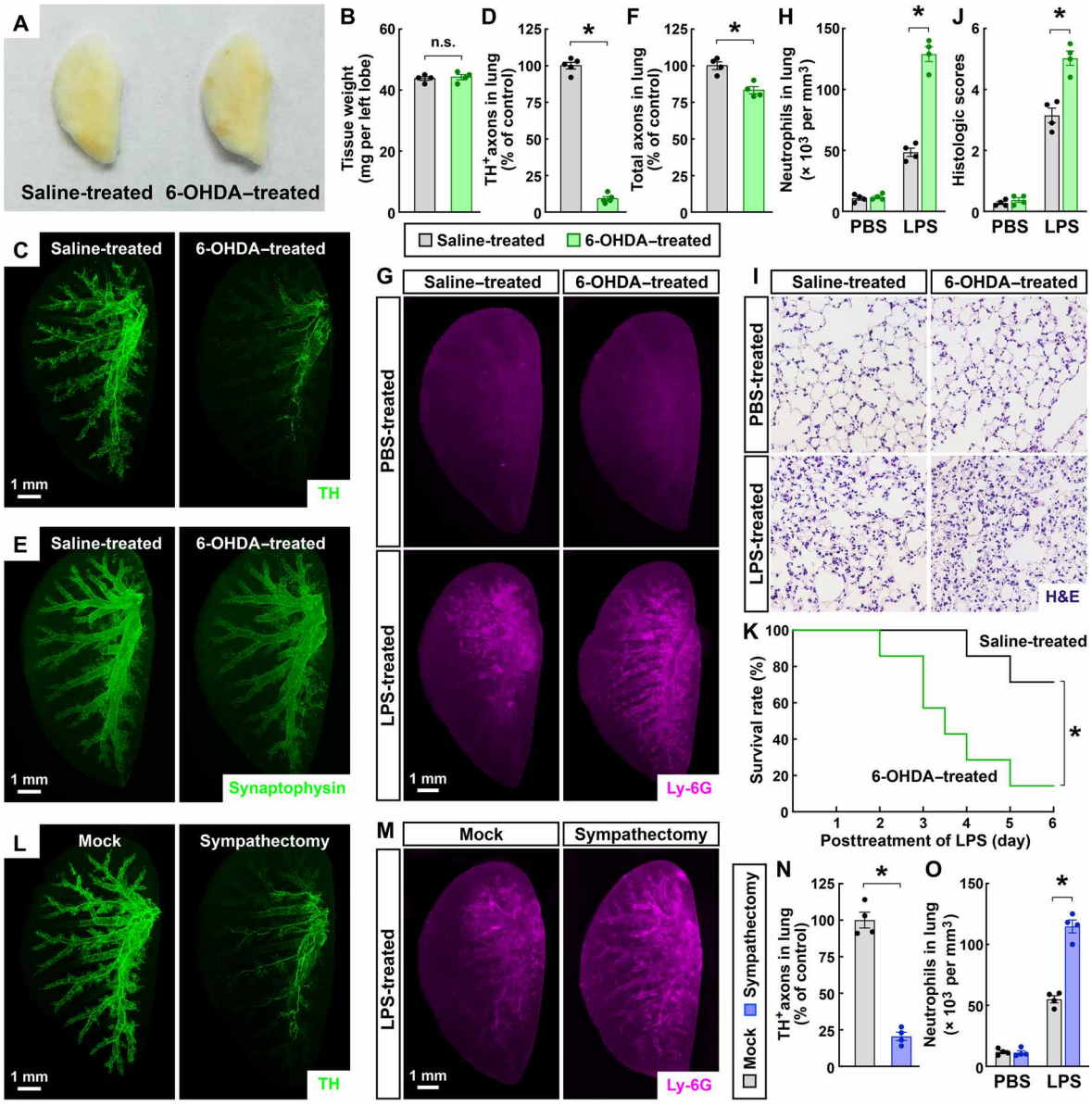

Fig. 3. Pharmacologic or surgical ablation of local sympathetic innervations enhanced the LPS-elicited immune response in the lung. (**A** to **F**) Pharmacologic ablation of local sympathetic innervations in the lung. The wild-type mice were intranasally treated with saline control or 6-OHDA. (A) Gross appearance of the lungs (left lobe) of saline-treated versus 6-OHDA–treated mice. Photo credit: Tingting Liu, Peking University. (B) The tissue weight of the lungs was quantified. $n = 4$, means ± SEM, n.s., not significant (Student's t test). (C to F) The lungs (left lobe) of saline-treated and 6-OHDA–treated mice were processed for the whole-tissue immunolabeling of anti-TH (C and D) or anti-synaptophysin (E and F). (C and E) Representative 3D projection images at ×1.26 magnification of the lightsheet imaging are shown. (D) TH-positive sympathetic axons were quantified. $n = 5$, means ± SEM, $^*P < 0.01$ (Student's t test). (F) Synaptophysin-positive total axons were quantified. $n = 4$, means ± SEM, $^*P < 0.01$ (Student's t test). (**G** to **K**) Pharmacologic ablation of local sympathetic innervations in the lung promoted the LPS-elicited immune response. Saline-treated and 6-OHDA–treated mice were intranasally administered with LPS. (G and H) The lungs (left lobe) were processed for the whole-tissue anti–Ly-6G immunolabeling. (G) Representative 3D projection images at ×1.26 magnification of the lightsheet imaging are shown. (H) The density of Ly-6G$^+$ neutrophils was quantified. $n = 4$, means ± SEM, $^*P < 0.01$ (ANOVA test). (I and J) The lung tissues were assessed by H&E staining. (I) Representative images are shown. (J) The histologic scores were determined. $n = 4$, means ± SEM, $^*P < 0.01$ (ANOVA test). (K) The survival rate of the mice was followed for 6 days after the LPS treatment. $n = 7$, $^*P < 0.05$ (log-rank test). (**L** and **N**) Surgical ablation of local sympathetic innervations in the lung. The wild-type mice were subjected to the local sympathectomy of the lung. The lungs (left lobe) of the mice after mock surgery or sympathectomy were processed for the whole-tissue anti-TH immunolabeling. (L) Representative 3D projection images at ×1.26 magnification of the lightsheet imaging are shown. (N) TH-positive sympathetic axons were quantified. $n = 4$, means ± SEM, $^*P < 0.01$ (Student's t test). (**M** and **O**) Surgical ablation of local sympathetic innervations in the lung enhanced the LPS-elicited immune response. The mice after mock surgery or sympathectomy were intranasally administered with LPS, and the lungs (left lobe) were then processed for the whole-tissue anti–Ly-6G immunolabeling. (M) Representative 3D projection images at ×1.26 magnification of the lightsheet imaging are shown. (O) The density of Ly-6G$^+$ neutrophils was quantified. $n = 4$, means ± SEM, $^*P < 0.01$ (ANOVA test).

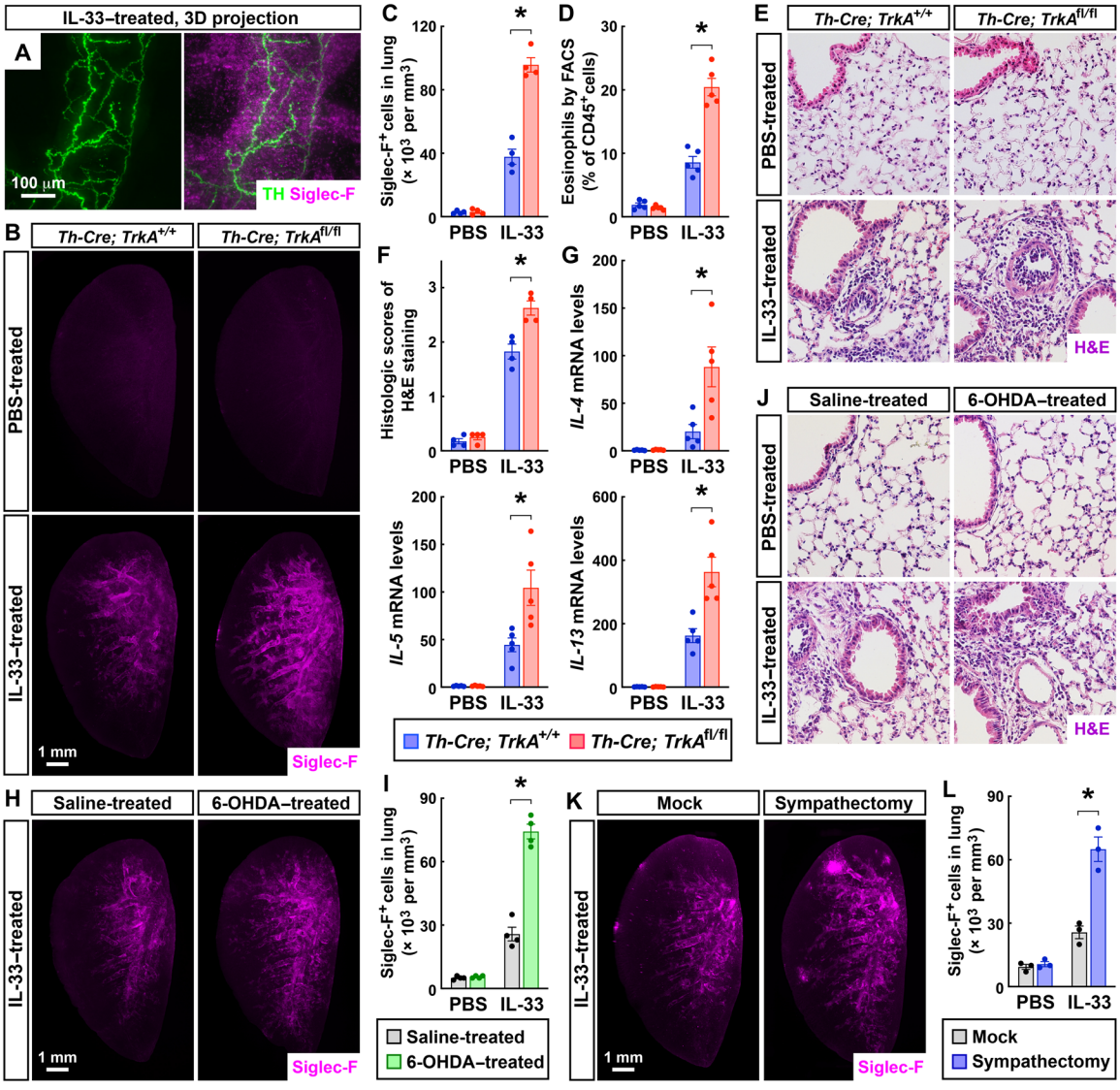

Fig. 4. Local sympathetic innervations negatively modulate the IL-33–elicited type 2 innate immunity in the lung. (**A**) Spatial engagement of local sympathetic innervations with the IL-33–elicited immune response in the lung. The wild-type mice were intranasally treated with IL-33. The lung (left lobe) was then processed for the whole-tissue coimmunolabeling of anti-TH (green) and anti–Siglec-F (magenta). Representative 3D projection images of the 600-μm depth of the intact tissue at ×12.6 magnification of the lightsheet imaging are shown. (**B** to **F**) Genetic ablation of local sympathetic innervations in the lung boosted the IL-33–elicited type 2 innate immunity. *Th-Cre; TrkA*$^{+/+}$ and *Th-Cre; TrkA*$^{fl/fl}$ mice were intranasally treated with saline control or IL-33. The lungs were harvested at 24 hours after the second instillation. (B and C) The lungs (left lobe) were processed for the whole-tissue anti–Siglec-F immunolabeling. (B) Representative 3D projection images at ×1.26 magnification of the lightsheet imaging are shown. (C) The density of Siglec-F$^+$ immune cells was quantified. $n = 4$, means ± SEM, $^*P < 0.01$ (ANOVA test). (D) CD45$^+$ CD11c$^-$ Siglec-F$^+$ eosinophils were quantified by the FACS analysis. $n = 5$, means ± SEM, $^*P < 0.01$ (ANOVA test). (E and F) The lung tissues were assessed by H&E staining. (E) Representative images are shown. (F) The histologic scores were determined. $n = 4$, means ± SEM, $^*P < 0.01$ (ANOVA test). (**G**) Local sympathetic innervations negatively regulate the IL-33–elicited early immune response. The lungs of *Th-Cre; TrkA*$^{+/+}$ and *Th-Cre; TrkA*$^{fl/fl}$ mice were harvested at 2 hours after the first instillation of IL-33. Expression levels of cytokines were determined by the qPCR analysis. $n = 5$, means ± SEM, $^*P < 0.01$ (ANOVA test). (**H** to **J**) Pharmacologic ablation of local sympathetic innervations in the lung enhanced the IL-33–elicited immune response. Saline-treated and 6-OHDA–treated mice were intranasally administered with IL-33. The lungs were harvested at 24 hours after the second instillation. (H and I) The lungs (left lobe) were processed for the whole-tissue anti–Siglec-F immunolabeling. (H) Representative 3D projection images at ×1.26 magnification of the lightsheet imaging are shown. (I) The density of Siglec-F$^+$ immune cells was quantified. $n = 4$, means ± SEM, $^*P < 0.01$ (ANOVA test). (J) The lung tissues were assessed by H&E staining, and representative images are shown. (**K** and **L**) Surgical ablation of local sympathetic innervations in the lung promoted the IL-33–elicited immune response. The wild-type mice after mock surgery or local sympathectomy were intranasally administered with IL-33. The lungs (left lobe) were harvested at 24 hours after the second instillation and processed for the whole-tissue anti–Siglec-F immunolabeling. (K) Representative 3D projection images at ×1.26 magnification of the lightsheet imaging are shown. (L) The density of Siglec-F$^+$ immune cells was quantified. $n = 3$, means ± SEM, $^*P < 0.01$ (ANOVA test).

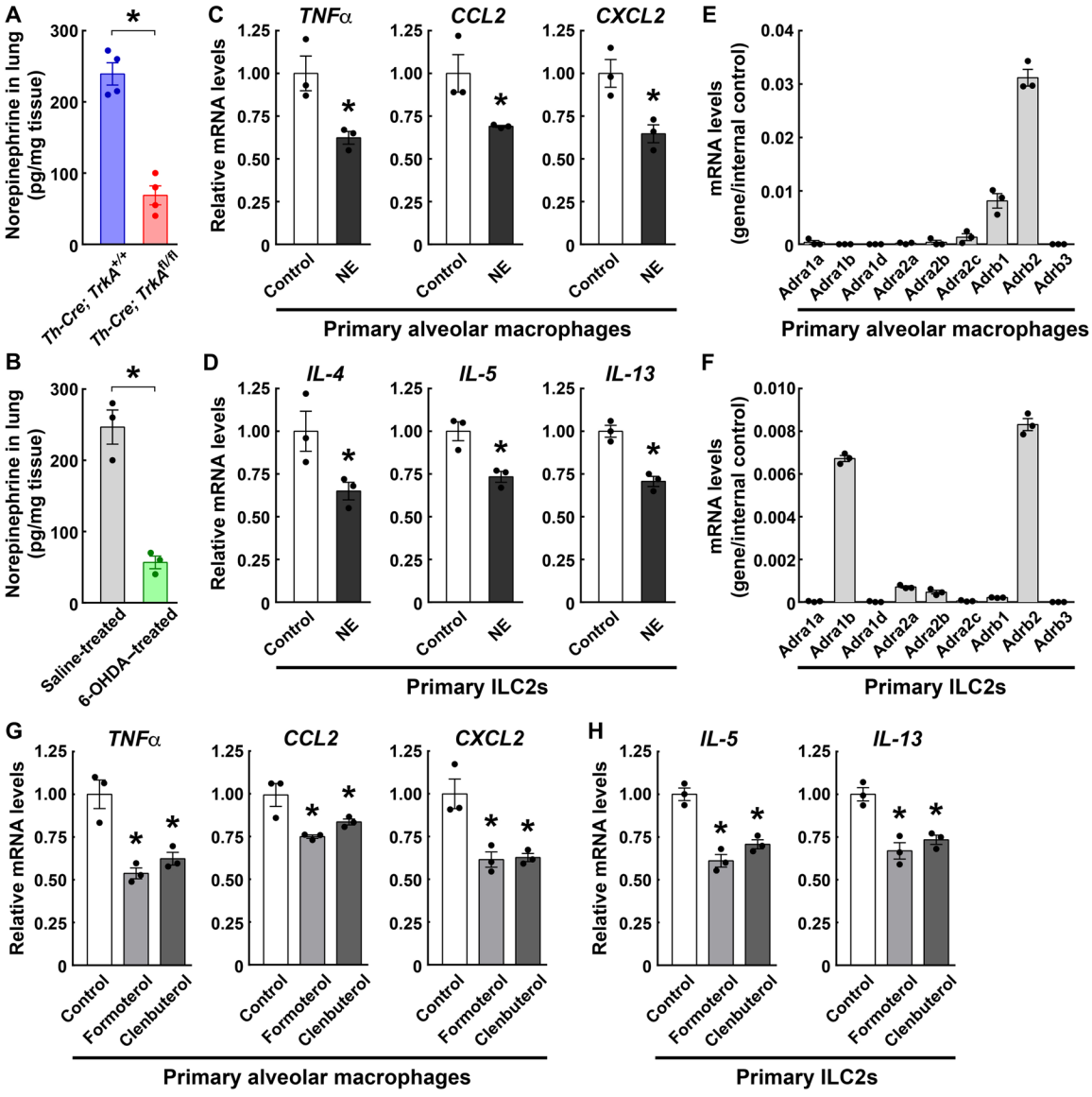

Fig. 5. Sympathetic neurotransmitter NE cell-intrinsically inhibits the innate immune responses. (**A**) Decrease in the NE content in the lungs of *Th-Cre; TrkA*$^{fl/fl}$ mice. $n = 4$, means ± SEM, *$P < 0.01$ (Student's t test). (**B**) Decrease in the NE content in the lungs of 6-OHDA–treated mice. $n = 3$, means ± SEM, *$P < 0.01$ (Student's t test). (**C** and **D**) NE cell-intrinsically suppressed the LPS- or IL-33–elicited innate immune response. Primary alveolar macrophages (C) or ILC2s (D) isolated from the lungs of wild-type mice were in vitro treated with LPS (C) or IL-33 (D) in the presence of 10 μM NE. Expression levels of cytokines and chemokines were examined by the qPCR analysis. $n = 3$, means ± SEM, *$P < 0.01$ (ANOVA test). (**E** and **F**) The expression profile of adrenergic receptors in primary alveolar macrophages (E) or ILC2s (F) was determined by the qPCR analysis. $n = 3$, means ± SEM. (**G** and **H**) β2-Adrenergic receptor signaling cell-intrinsically inhibited the LPS- or IL-33–elicited innate immune response. Primary alveolar macrophages (G) or ILC2s (H) were in vitro treated with LPS or IL-33 in the presence of 10 μM formoterol or clenbuterol. Expression levels of cytokines and chemokines were examined by the qPCR analysis. $n = 3$, means ± SEM, *$P < 0.01$ (ANOVA test).

the LPS- or IL-33–elicited innate immunity in specific types of immune cells.

We next investigated the downstream signal involved in these immunomodulatory actions of NE. We examined the expression profile of α- and β-adrenergic receptors and revealed that the β2-adrenergic receptor (*Adrb2*) was the most highly expressed one in primary alveolar macrophages (Fig. 5E). Similarly, *Adrb2* showed the highest expression level in primary ILC2s isolated from the lungs (Fig. 5F). Therefore, we tested whether the β2-adrenergic receptor signal would participate in the immunomodulatory function in primary alveolar macrophages or ILC2s. The in vitro treatment of alveolar macrophages with formoterol or clenbuterol, the two specific agonists for the β2-adrenergic receptor, effectively dampened the LPS-elicited expression of *TNFα*, *CCL2*, and *CXCL2* (Fig. 5G). In addition, the in vitro treatment of ILC2s with formoterol or clenbuterol decreased the IL-33–elicited expression of *IL-5* and *IL-13* (Fig. 5H). These results indicated that the β-adrenergic receptor signal could negatively regulate the LPS- or IL-33–elicited innate immune response, in accordance with the previous reports that activation of the β2-adrenergic receptor suppressed the immune

function of macrophages or ILC2s, as well as the lung inflammation (*38*, *39*).

We further examined the lung innate immunity in the mice with genetic deletion of the β2-adrenergic receptor. *Adrb2*$^{-/-}$ mice had the normal development of local sympathetic innervations in the lungs, as assessed by the whole-tissue anti-TH immunolabeling (Fig. 6, A and B). However, we observed that the LPS-elicited neutrophil recruitment was significantly stronger in the *Adrb2*$^{-/-}$ lungs than that in the *Adrb2*$^{+/+}$ lungs, as visualized by the anti–Ly-6G immunolabeling (Fig. 6, C and D). This increased neutrophil recruitment in *Adrb2*$^{-/-}$ lungs could be thwarted by the intravenous administration of anti-CXCL2 neutralizing antibody (fig. S5F). In addition, the FACS analysis revealed more accumulation of neutrophils in the BALF of the *Adrb2*$^{-/-}$ lungs (Fig. 6E). On the other hand, we detected the comparable profiles of alveolar macrophages and interstitial macrophages in *Adrb2*$^{+/+}$ and *Adrb2*$^{-/-}$ lungs in response to LPS (fig. S6, A and B). Moreover, *Adrb2*$^{-/-}$ mice showed the exacerbated histopathology in the lungs (Fig. 6, F and G), as well as the compromised survival after the LPS treatment (Fig. 6H), similar to the above observations with the local sympathetic ablation. To further rule out that the enhancement of LPS-elicited immune response might be due to any developmental issue in *Adrb2*$^{-/-}$ mice, we used ICI-118,551, the specific antagonist of the β2-adrenergic receptor. The intranasal delivery of ICI-118,551 was sufficient to boost the LPS-elicited neutrophil recruitment (fig. S6, C and D), supporting the specific function of the β2-adrenergic receptor signal in negatively controlling the LPS-elicited immune response in the lung.

In addition, resembling the immunomodulatory effects with the local sympathetic ablation, the IL-33–elicited accumulation of Siglec-F^{+} immune cells was higher in *Adrb2*$^{-/-}$ lungs (Fig. 6, I and J). Also, the

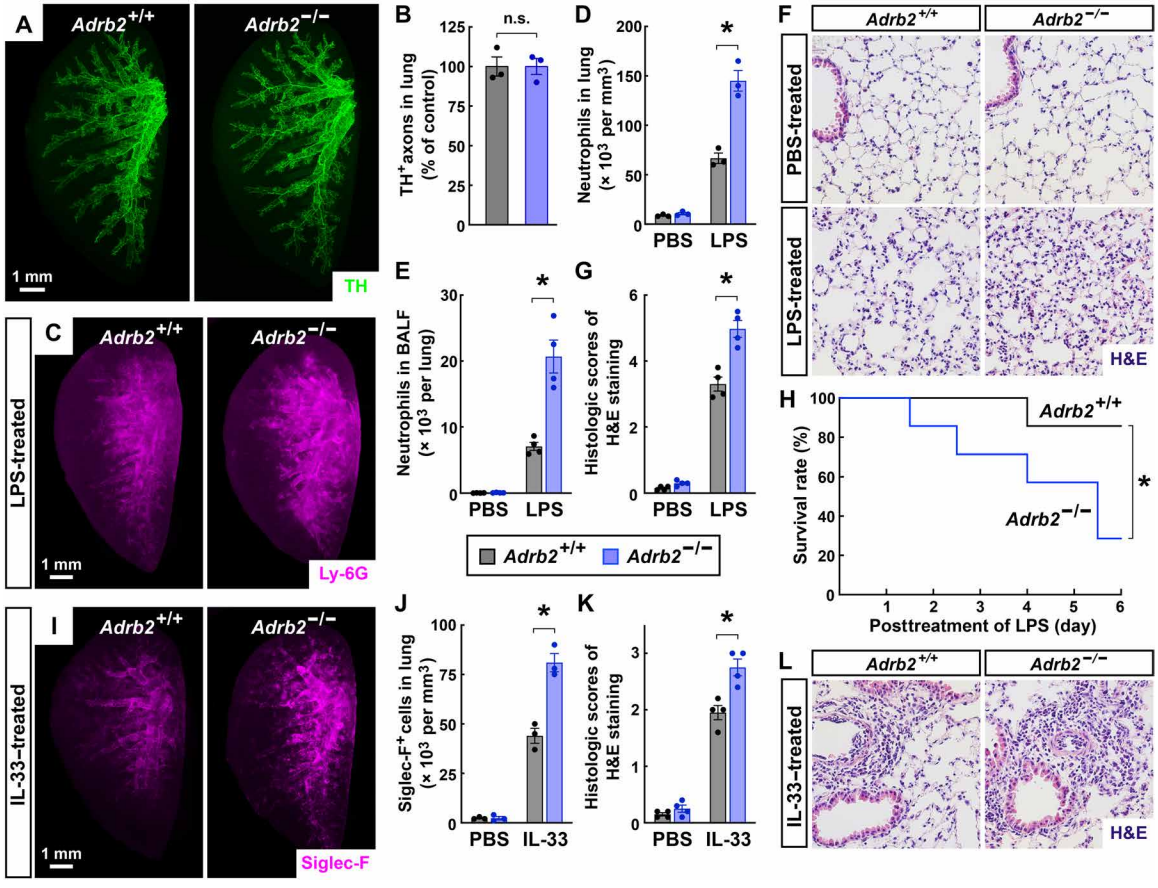

Fig. 6. β2-Adrenergic receptor signaling suppresses the innate immune responses in the lung. (**A** and **B**) Normal development of local sympathetic innervations in the lungs of *Adrb2*$^{-/-}$ mice. The lungs (left lobe) of *Adrb2*$^{+/+}$ and *Adrb2*$^{-/-}$ mice were processed for the whole-tissue anti-TH immunolabeling. (A) Representative 3D projection images at ×1.26 magnification of the lightsheet imaging are shown. (B) TH-positive sympathetic axons were quantified. $n = 3$, means ± SEM, $^{*}P < 0.01$ (Student's *t* test). (**C** to **H**) Genetic deletion of the β2-adrenergic receptor boosted the LPS-elicited immune response. *Adrb2*$^{+/+}$ and *Adrb2*$^{-/-}$ mice were intranasally treated with saline control or LPS. (C and D) The lungs (left lobe) were processed for the whole-tissue anti–Ly-6G immunolabeling. (C) Representative 3D projection images at ×1.26 magnification of the lightsheet imaging are shown. (D) The density of Ly-6G^{+} neutrophils was quantified. $n = 3$, means ± SEM, $^{*}P < 0.01$ (ANOVA test). (E) CD45^{+} CD11b^{+} Ly-6G^{+} neutrophils in the BALF were quantified by the FACS analysis. $n = 4$, means ± SEM, $^{*}P < 0.01$ (ANOVA test). (F and G) The lung tissues were assessed by H&E staining. (F) Representative images are shown. (G) The histologic scores were determined. $n = 4$, means ± SEM, $^{*}P < 0.01$ (ANOVA test). (H) The survival rate of the mice was followed for 6 days after the LPS treatment. $n = 7$, $^{*}P < 0.05$ (log-rank test). (**I** to **L**) Genetic deletion of the β2-adrenergic receptor enhanced the IL-33–elicited immune response in the lung. *Adrb2*$^{+/+}$ and *Adrb2*$^{-/-}$ mice were intranasally treated with saline control or IL-33. (I and J) The lungs (left lobe) were processed for the whole-tissue anti–Siglec-F immunolabeling. (I) Representative 3D projection images at ×1.26 magnification of the lightsheet imaging are shown. (J) The density of Siglec-F^{+} immune cells was quantified. $n = 3$, means ± SEM, $^{*}P < 0.01$ (ANOVA test). (K and L) The lung tissues were assessed by H&E staining. (L) Representative images are shown. (K) The histologic scores were determined. $n = 4$, means ± SEM, $^{*}P < 0.01$ (ANOVA test).

histopathology after the IL-33 treatment became more profound in *Adrb2*$^{-/-}$ lungs (Fig. 6, K and L). Furthermore, the intranasal administration of ICI-118,551 could effectively promote the IL-33–elicited accumulation of Siglec-F^{+} immune cells in the lungs (fig. S6, E and F). These results, in line with the recent report (*39*), confirm that the β2-adrenergic receptor signal negatively modulates the IL-33–elicited type 2 innate immunity in the lung.

DISCUSSION

In this study, we developed the iDISCO(ace) procedure for robust whole-tissue immunolabeling and 3D fluorescence imaging of the intact lung tissues. The capabilities of this technique overcome the intrinsic limitations of conventional immunohistochemistry in assessing the 3D distribution of cellular structures, which enabled us to visualize different types of local neural innervations in the lung on the whole-tissue level. In addition, iDISCO(ace) exhibits better antibody compatibility, especially for surface epitopes of immune cell markers, compared with the original iDISCO^{+} method (*19*). Therefore, this technical advance could apply to many areas of lung research and is poised to serve the field in future investigations on different aspects of this vital organ.

A previous report showed that pharmacologic activation of the β2-adrenergic receptor in macrophages could dampen the LPS-elicited immune response in the lung (*38*). Other recent work reported that the β2-adrenergic receptor signal inhibited the function of ILC2s, with its genetic deletion boosting the type 2 innate immunity in the lung (*39*). Our observations with the specific agonists for the β2-adrenergic receptor, as well as *Adrb2*$^{-/-}$ mice, are in line with these previous studies. However, we went further to demonstrate that genetic, pharmacologic, or surgical ablation of sympathetic innervations in the lung promoted both the LPS- or IL-33–elicited immune response. These results have convincingly supported the conclusion that the sympathetic signal can modulate lung innate immunity by a local, direct mechanism. Notably, one of the conventional treatments for asthma and other pulmonary diseases is the administration of short- or long-acting β2-agonists (*40*–*42*). It has been the canonical view that these β2-agonists act as bronchodilators. However, the findings by our colleagues and this current study have collectively suggested the possibility that β2-agonists could mitigate the pulmonary diseases through a beneficial immunomodulatory effect in addition to dilating the airways. More detailed studies are warranted to fully understand the mechanism of action of these commonly prescribed β2-agonists.

Our study has elucidated a previously unappreciated function of local sympathetic innervations in the lung, but important questions remain to be addressed by future research. First, how the local sympathetic signal would affect other types of immune cells, e.g., dendritic cells, natural killer cells, and T cells, in the lung immunity is unclear. The sympathetic neurotransmitter NE might broadly suppress different types of immune cells, similar to its function on alveolar macrophages and ILC2s. Alternatively, NE might have an opposite, stimulatory role for specific immune cells, which could conceivably be due to their distinct expression profile of adrenergic receptors. Second, how local parasympathetic innervations, whose density is much higher than that of sympathetic innervations, would influence lung immune responses is mostly uncharted. A prior study reported that the parasympathetic signal facilitated spontaneous pneumonia after stroke (*16*). It will be interesting to examine the balance of the immunomodulatory effects afforded by the sympathetic and parasympathetic signals. Third, how the nervous system would respond to physiological or pathological cues in tuning the lung immunity remains intriguingly unknown. It will be instructive to determine the neural circuitries of the peripheral and central nervous systems that bridge the local afferent and efferent neural signals in the lung. A recent study showed that the nociceptor sensory innervations inhibited the antibacterial immune response in the lung by releasing the neuropeptide CGRP (*17*). It appears possible that these sensory innervations might also relay the afferent signal from the lung to the putative neural circuitries for controlling the efferent sympathetic signal, whose immunomodulatory function has been uncovered here.

In summary, this study has reported the critical function of local sympathetic innervations in modulating the lung innate immunity, which would have important implications in our better understanding of the neuroimmune interplay in homeostasis and disease of the lung.

MATERIALS AND METHODS

iDISCO(ace) procedure

The iDISCO(ace) protocol was developed as a modification of the original iDISCO^{+} method (*19*). This procedure enables the whole-tissue immunolabeling and 3D assessment of intended cellular structures, including but not limited to neural innervations, neuroendocrine cells, lymphatic vessels, and different immune cells, in the unsectioned lung tissues. The anesthetized mice were perfused sequentially with 20 ml of phosphate-buffered saline (PBS)/heparin (100 μg/ml) and 20 ml of PBS/1% paraformaldehyde (PFA)/10% sucrose/heparin (100 μg/ml). The lung tissues were dissected out and postfixed in PBS/0.5% PFA at room temperature for 2 hours. The tissues were washed with PBS at room temperature for 30 min twice. All the incubation steps were performed with gentle rotating.

The lung tissues were treated at room temperature with 25% acetone (diluted in ddH_2O) for 1 hour, 50% acetone for 3 hours, and 25% acetone for 1 hour. The tissues were washed with PBS at room temperature for 30 min twice, followed by PBS/30% sucrose for 2 hours. The tissues were decolorized in PBS/30% sucrose/1% H_2O_2/10 mM EDTA-Na (pH 8.0) at 4°C overnight. The tissues were then washed with PBS at room temperature for 30 min twice, followed by PBS/0.2% Triton X-100/0.1% deoxycholate/10% DMSO/10 mM EDTA (pH 8.0) overnight. All the incubation steps were performed with gentle rotating.

Next, the tissues were blocked with PBS/0.2% Triton X-100/10% DMSO/5% normal donkey serum at room temperature overnight and then immunolabeled with intended primary antibodies (1:500 dilution) in PBS/0.1% Tween 20/heparin (10 μg/ml)/5% normal donkey serum at room temperature for 48 hours. The primary antibodies used in this study were rabbit anti-synaptophysin (Thermo Fisher Scientific, catalog no. 180130, RRID:AB_10836766), rabbit anti-Tuj1 (Covance, catalog no. MRB-435P, RRID:AB_663339), rabbit anti-PGP9.5 (ProteinTech Group, catalog no. 14730-1-AP, RRID:AB_2210497), rabbit anti-TH (Millipore, catalog no. AB152, RRID:AB_390204), goat anti-VChAT (Millipore, catalog no. ABN100, RRID:AB_2630394), goat anti-CGRP (Abcam, catalog no. ab36001, RRID:AB_725807), rat anti-LYVE1 (Thermo Fisher Scientific, catalog no. 14-0443-82, RRID:AB_1633414), rat anti-CD3 (BioLegend, catalog no. 100202, RRID:AB_312659), rat anti-CD11b (BioLegend, catalog no. 101202, RRID:AB_312785), rat anti–Siglec-F (BD Biosciences, catalog no. 552125, RRID:AB_394340), rat anti–Ly-6G (Thermo Fisher Scientific, catalog

no. 16-9668-85, RRID:AB_2573127), and rat anti-F4/80 (BioLegend, catalog no. 123102, RRID:AB_893506). The tissues were washed with PBS/0.1% Tween 20/heparin (10 μg/ml) at room temperature for 12 hours, with the fresh buffer changed every 2 hours. The tissues were further immunolabeled with the corresponding Alexa Fluor dye–conjugated secondary antibodies (1:500 dilution; Thermo Fisher Scientific) in PBS/0.1% Tween 20/heparin (10 μg/ml)/5% normal donkey serum at room temperature for 48 hours. The tissues were washed with PBS/0.1% Tween 20/heparin (10 μg/ml) at room temperature for 24 hours, with the fresh buffer changed every 6 hours. All the incubation steps were performed with gentle rotating.

The immunolabeled lung tissues were washed with PBS at room temperature for 2 hours and embedded in PBS/0.8% agarose before the optical clearing. The tissue blocks were incubated at room temperature with 20% methanol (diluted in ddH_2O) for 1 hour three times, 40% methanol for 1 hour, 60% methanol for 1 hour, 80% methanol for 1 hour, 100% methanol for 1 hour, and 100% methanol overnight. The tissue blocks were then incubated at room temperature with the mixture of dichloromethane and methanol (2:1) for 3 hours, followed by 100% dichloromethane for 30 min three times. The tissue blocks were lastly incubated at room temperature with 100% dibenzyl ether for 12 hours twice. All the incubation steps were performed with gentle rotating.

Lightsheet imaging

The lung tissues processed by the iDISCO(ace) procedure were imaged on a LaVision BioTec UltraMicroscope II equipped with the scientific complementary metal-oxide semiconductor (sCMOS) camera (Andor Neo) and a 2×/NA 0.5 objective (MVPLAPO) covered with a 10-mm working distance dipping cap. The tissues were immersed in an imaging chamber filled with 100% dibenzyl ether. For imaging at ×1.26 (0.63× zoom) magnification, each tissue was scanned by three combined lightsheets from the left side with a step size of 3 μm. For imaging at ×12.6 magnification (6.3× zoom), each tissue was scanned by a single lightsheet (middle position) from the left side with a step size of 1 μm. The image stacks were acquired by the continuous lightsheet scanning method without the contrast-blending algorithm.

Imaris (https://imaris.oxinst.com/packages) was used to reconstruct the image stacks obtained from the lightsheet imaging. For the purpose of display in figures and movies, a gamma correction of 1.3 to 1.6 was applied to the raw data. Orthogonal projections of the image stacks were generated for the representative 3D images shown in the figures. The movies were produced with a constant frame rate of 30 frames per second.

Animals

All experimental procedures in mice were performed in compliance with the protocol approved by the Institutional Animal Care and Use Committee (IACUC) of Peking University. The macaque lung tissues were collected from 5-year-old male monkeys in compliance with the protocol approved by the IACUC of Kunming Institute of Zoology, Chinese Academy of Sciences.

The mice used in the experiments were 8- to 12-week-old males unless otherwise specified. C57BL/6 wild-type mice were purchased from Charles River International. *Th-Cre* (JAX 008601, RRID:IMSR_JAX:008601) and $TrkA^{fl/fl}$ (JAX 022362, RRID:IMSR_JAX:022362) were bred in-house to generate the littermates for experiments. $Adrb1^{-/-}$; $Adrb2^{-/-}$ (JAX 003810, RRID:IMSR_JAX:003810) was backcrossed with C57BL/6 wild-type mice for two generations to obtain $Adrb2^{+/-}$ mice, which were further bred to generate the littermates for experiments.

For all intranasal administrations, the mice were briefly anesthetized with 3% isoflurane. For papain treatment, 25 μg of papain (dissolved in 40 μl of sterile PBS; Sigma-Aldrich) per mouse was administered daily by intranasal instillation for 4 days, and the lung tissues were harvested at 24 hours after the last instillation. For the chitin treatment, chitin beads (New England Biolabs) were washed with sterile PBS three times, and large aggregates were settled for 2 min. Chitin beads in suspension were counted by a hemocytometer and then adjusted to a final concentration of 1×10^5 chitin beads/ml in sterile PBS. Five thousand chitin beads (in 50 μl of sterile PBS) per mouse were administered daily for 3 days, and the lung tissues were harvested at 24 hours after the last instillation. For tissue analyses after the LPS treatment, 0.5 μg of LPS (dissolved in 40 μl of sterile PBS; Sigma-Aldrich) per mouse was administered, and the lung tissues were harvested at 2 hours after the instillation. For survival experiments after the LPS treatment, 450 μg of LPS (dissolved in 45 μl of sterile PBS) per mouse was administered, and the mice were monitored for 6 days. For the IL-33 treatment, 3 μg of recombinant mouse IL-33 (dissolved in 40 μl of sterile PBS; PeproTech) per mouse was administered daily for 2 days, and the lung tissues were harvested at 24 hours after the second instillation. For the specific antagonist of the β2-adrenergic receptor ICI-118,551, 200 μg of ICI-118,551 (dissolved in 10 μl of sterile PBS; Selleckchem) per mouse was administered in combination with the LPS or IL-33 treatment. For the 6-OHDA treatment, 500 μg of 6-OHDA (dissolved in 50 μl of sterile PBS containing 0.1% ascorbic acid; Sigma-Aldrich) per mouse was administered daily for 3 days, and the mice were then used for experiments at 3 days after the last instillation.

For treatment with anti-CXCL2 neutralizing antibody (Thermo Fisher Scientific, catalog no. MA5-23737, RRID:AB_2609513), the mice were intravenously injected with control immunoglobulin G or anti-CXCL2 at 2 mg/kg of body weight. The mice were then used for experiments at 1 hour after the antibody injection.

For local sympathectomy of the lung, wild-type mice were anesthetized with 2.5% isoflurane and supported by a rodent ventilator. The skin from the neck to the chest region was shaved and prepared with iodine and alcohol. An incision on the skin was made along the midline, followed by the thoracotomy to the second rib level. Fat tissues surrounding the aortic arch were carefully separated to expose the underneath pulmonary plexus. The sympathetic branches entering the pulmonary plexus were cut by a pair of fine scissors. The rib cage and the overlying skin were then brought back into the original anatomical position and sutured. The mice were used for experiments at 10 days after the surgery.

Tissue analyses

For FACS analysis of the lung tissues, the tissues were acutely dissected out and cut into small pieces on ice with a pair of scissors. The tissues were digested at 37°C for 15 min in RPMI 1640 medium containing Liberase (0.1 mg/ml; Roche)/deoxyribonuclease I (20 μg/ml; Sigma-Aldrich)/10 mM Hepes/3% heat-inactivated fetal bovine serum (Sigma-Aldrich) and then mashed through 70-μm cell strainers. The cells were stained with intended FACS antibodies and processed on the BD LSRFortessa. For the FACS analysis of immune cells in the BALF, 1 ml of RPMI 1640 medium containing 3% heat-inactivated fetal bovine serum was gently infused into the lungs of euthanized

mice through the esophagus with a 1-ml insulin syringe and then aspirated back to collect the cells in the BALF. The cells were stained with intended FACS antibodies and processed on the BD LSRFortessa. The FACS data were analyzed by FlowJo (https://www.flowjo.com).

For the quantitative polymerase chain reaction (qPCR) analysis, the lung tissues were acutely dissected out. Total RNAs were extracted by the RNeasy Mini Kit (Qiagen) and analyzed by the SYBR Green Real-Time PCR Kit (Thermo Fisher Scientific).

The whole-tissue immunolabeling and 3D imaging of sympathetic innervations in the femur were performed according to the BoneClear method, as we recently described (*31*). The whole-tissue immunolabeling and 3D imaging of sympathetic innervations in the spleen, thymus, and lymph node were performed according to the ImmuView method as reported (*30*).

In vitro treatments

For the in vitro treatment of primary alveolar macrophages, 1 ml of Dulbecco's modified Eagle's medium (DMEM) containing 10% heat-inactivated fetal bovine serum/penicillin (100 U/ml)/streptomycin (100 μg/ml) was gently infused into the lungs of euthanized wild-type mice through the esophagus with a 1-ml insulin syringe and then aspirated back to collect alveolar macrophages. Primary alveolar macrophages were rested at 37°C overnight before indicated treatments.

For the in vitro treatment of primary ILC2s, the wild-type mice were intranasally administered with recombinant IL-33 as described above. Primary ILC2s [$CD45^+$ $CD90.2^+$ Lin^-; Lin^-: $CD3^-$ $CD4^-$ $CD8a^-$ $TCR\beta^-$ $TCR\gamma\delta^-$ $CD19^-$ $Gr1^-$ $CD11b^-$ $CD11c^-$ $NK1.1^-$ $TER119^-$] in the lungs were FACS sorted on the BD FACSAria (BD Biosciences). Primary ILC2s were rested in DMEM containing 20% heat-inactivated fetal bovine serum/penicillin (100 U/ml)/streptomycin (100 μg/ml) at 37°C for 6 hours before indicated treatments. For the qPCR analysis, total RNAs were extracted from alveolar macrophages or ILC2s by the RNeasy Mini Kit and analyzed by the SYBR Green Real-Time PCR Kit.

NE measurement

Measurement of the NE content was performed by the Metabolomics Facility at the Technology Center for Protein Sciences of Tsinghua University. The lung tissues were acutely dissected out from the mice of indicated conditions and immediately quenched in 80% methanol prechilled at −80°C. The tissues were homogenized on dry ice and then stored at −80°C for 2 hours. The mixtures were centrifuged at 4°C for 20 min to pellet the tissue debris, and the supernatants were dried in a SpeedVac.

The samples were analyzed on the Dionex Ultimate 3000 Ultraperformance Liquid Chromatography System coupled to the TSQ Quantiva Ultra Triple-Quadrupole Mass Spectrometer with a heated electrospray ionization probe in the positive ion mode. The BEH amide column (Waters) was used to separate the samples. Mobile phase A: 95% acetonitrile/5% ddH_2O/10 mM ammonium formate at pH 3.0 (adjusted by formate); mobile phase B: 50% acetonitrile/50% ddH_2O/10 mM ammonium formate at pH 3.0 (adjusted by formate); and linear gradient: 0 min, 2% B; 1.2 min, 2% B; 4.5 min, 98% B; 6 min, 98% B; 6.1 min, 2% B; and 8 min, 2% B.

Data were acquired in the selected reaction monitoring for NE with the transition of 170/107. Both the precursor and its fragment ion were collected with a resolution of 0.7 full width at half maximum. Spray voltage was 3500 V; ion transfer tube temperature, 350°C; vaporizer temperature, 300°C; sheath gas flow rate, 30 Arb; auxiliary gas flow rate, 10 Arb; collision-induced dissociation gas, 1.5 mtorr. Analysis and quantification were performed by Xcalibur 3.0.63 supported by Thermo Fisher Scientific.

Statistical methods

To quantify neural innervations in the lung, four 300 μm × 300 μm × 300 μm cubic volumes were randomly selected along the tertiary bronchi from the reconstructed 3D images of each tissue. Synaptophysin-positive total axons, TH-positive sympathetic axons, VChAT-positive parasympathetic axons, or CGRP-positive sensory axons in each cubic volume were manually traced.

To quantify the density of immune cells, three 300 μm × 300 μm × 300 μm cubic volumes were randomly selected along the tertiary bronchi from the reconstructed 3D images of each tissue. Ly-$6G^+$ neutrophils or Siglec-F^+ immune cells in each cubic volume were manually counted.

Histologic scoring of LPS-treated lung tissues was performed following the established standard (*43*) with modifications. Ten examined areas (×20 magnification) were randomly selected from the H&E sections of each tissue. Three parameters were scored and summed for each area: (i) neutrophils in the alveolar space: 0, none; 1, one to five neutrophils; and 2, more than five neutrophils; (ii) neutrophils in the interstitial space: 0, none; 1, one to five neutrophils; and 2, more than five neutrophils; and (iii) proteinaceous debris filling the airspaces: 0, none; 1, one debris; and 2, more than one debris.

Histologic scoring of IL-33–treated lung tissues was performed according to the reported criteria (*44*) with minor modifications. Ten examined areas (×20 magnification) were randomly selected from the H&E sections of each tissue: 0, no sign of cellular infiltration; 1, cellular infiltration in <10% of vessels and airways in each area; 2, cellular infiltration surrounding 10 to 50% of vessels and airways in each area; and 3, cellular infiltration surrounding >80% of vessels and airways in each area.

Student's *t* test, analysis of variance (ANOVA) test, or log-rank test was performed using GraphPad Prism (http://www.graphpad.com/scientific-software/prism). Statistical details of the experiments are included in the figure legends.

SUPPLEMENTARY MATERIALS

Supplementary material for this article is available at http://advances.sciencemag.org/cgi/content/full/6/20/eaay1497/DC1

View/request a protocol for this paper from *Bio-protocol*.

REFERENCES AND NOTES

1. A. Ray, K. Gulati, N. Rai, Stress, anxiety, and immunomodulation. *Vitam. Horm.* **103**, 1–25 (2017).
2. J. Ordovas-Montanes, S. Rakoff-Nahoum, S. Huang, L. Riol-Blanco, O. Barreiro, U. H. von Andrian, The regulation of immunological processes by peripheral neurons in homeostasis and disease. *Trends Immunol.* **36**, 578–604 (2015).
3. S. Talbot, S. L. Foster, C. J. Woolf, Neuroimmunity: Physiology and pathology. *Annu. Rev. Immunol.* **34**, 421–447 (2016).
4. S. S. Chavan, V. A. Pavlov, K. J. Tracey, Mechanisms and therapeutic relevance of neuro-immune communication. *Immunity* **46**, 927–942 (2017).
5. L. C. Rankin, D. Artis, Beyond host defense: Emerging functions of the immune system in regulating complex tissue physiology. *Cell* **173**, 554–567 (2018).
6. P. J. Barnes, Immunology of asthma and chronic obstructive pulmonary disease. *Nat. Rev. Immunol.* **8**, 183–192 (2008).
7. J. A. McCullers, The co-pathogenesis of influenza viruses with bacteria in the lung. *Nat. Rev. Microbiol.* **12**, 252–262 (2014).
8. P. J. Barnes, P. G. Burney, E. K. Silverman, B. R. Celli, J. Vestbo, J. A. Wedzicha, E. F. Wouters, Chronic obstructive pulmonary disease. *Nat. Rev. Dis. Primers.* **1**, 15076 (2015).

9. C. M. Lloyd, C. M. Hawrylowicz, Regulatory T cells in asthma. *Immunity* **31**, 438–449 (2009).
10. K. Chen, J. K. Kolls, T cell-mediated host immune defenses in the lung. *Annu. Rev. Immunol.* **31**, 605–633 (2013).
11. S. Epelman, K. J. Lavine, G. J. Randolph, Origin and functions of tissue macrophages. *Immunity* **41**, 21–35 (2014).
12. I. Martinez-Gonzalez, C. A. Steer, F. Takei, Lung ILC2s link innate and adaptive responses in allergic inflammation. *Trends Immunol.* **36**, 189–195 (2015).
13. R. N. Germain, Y. Huang, ILC2s - resident lymphocytes pre-adapted to a specific tissue or migratory effectors that adapt to where they move? *Curr. Opin. Immunol.* **56**, 76–81 (2018).
14. S. B. Mazzone, B. J. Canning, Autonomic neural control of the airways. *Handb. Clin. Neurol.* **117**, 215–228 (2013).
15. R. B. Chang, D. E. Strochlic, E. K. Williams, B. D. Umans, S. D. Liberles, Vagal sensory neuron subtypes that differentially control breathing. *Cell* **161**, 622–633 (2015).
16. O. Engel, L. Akyüz, A. C. da Costa Goncalves, K. Winek, C. Dames, M. Thielke, S. Herold, C. Böttcher, J. Priller, H. D. Volk, U. Dirnagl, C. Meisel, A. Meisel, Cholinergic pathway suppresses pulmonary innate immunity facilitating pneumonia after stroke. *Stroke* **46**, 3232–3240 (2015).
17. P. Baral, B. D. Umans, L. Li, A. Wallrapp, M. Bist, T. Kirschbaum, Y. Wei, Y. Zhou, V. K. Kuchroo, P. R. Burkett, B. G. Yipp, S. D. Liberles, I. M. Chiu, Nociceptor sensory neurons suppress neutrophil and γδ T cell responses in bacterial lung infections and lethal pneumonia. *Nat. Med.* **24**, 417–426 (2018).
18. K. Chung, J. Wallace, S. Y. Kim, S. Kalyanasundaram, A. S. Andalman, T. J. Davidson, J. J. Mirzabekov, K. A. Zalocusky, J. Mattis, A. K. Denisin, S. Pak, H. Bernstein, C. Ramakrishnan, L. Grosenick, V. Gradinaru, K. Deisseroth, Structural and molecular interrogation of intact biological systems. *Nature* **497**, 332–337 (2013).
19. N. Renier, E. L. Adams, C. Kirst, Z. Wu, R. Azevedo, J. Kohl, A. E. Autry, L. Kadiri, K. Umadevi Venkataraju, Y. Zhou, V. X. Wang, C. Y. Tang, O. Olsen, C. Dulac, P. Osten, M. Tessier-Lavigne, Mapping of brain activity by automated volume analysis of immediate early genes. *Cell* **165**, 1789–1802 (2016).
20. E. A. Susaki, K. Tainaka, D. Perrin, F. Kishino, T. Tawara, T. M. Watanabe, C. Yokoyama, H. Onoe, M. Eguchi, S. Yamaguchi, T. Abe, H. Kiyonari, Y. Shimizu, A. Miyawaki, H. Yokota, H. R. Ueda, Whole-brain imaging with single-cell resolution using chemical cocktails and computational analysis. *Cell* **157**, 726–739 (2014).
21. W. Li, R. N. Germain, M. Y. Gerner, Multiplex, quantitative cellular analysis in large tissue volumes with clearing-enhanced 3D microscopy (C_e3D). *Proc. Natl. Acad. Sci. U.S.A.* **114**, E7321–E7330 (2017).
22. A. G. Pearse, Common cytochemical and ultrastructural characteristics of cells producing polypeptide hormones (the APUD series) and their relevance to thyroid and ultimobranchial C cells and calcitonin. *Proc. R. Soc. Lond. B Biol. Sci.* **170**, 71–80 (1968).
23. A. G. Pearse, The cytochemistry and ultrastructure of polypeptide hormone-producing cells of the APUD series and the embryologic, physiologic and pathologic implications of the concept. *J. Histochem. Cytochem.* **17**, 303–313 (1969).
24. D. E. Niewoehner, J. Kleinerman, Effects of experimental emphysema and bronchiolitis on lung mechanics and morphometry. *J. Appl. Physiol.* **35**, 25–31 (1973).
25. T. A. Reese, H. E. Liang, A. M. Tager, A. D. Luster, N. van Rooijen, D. Voehringer, R. M. Locksley, Chitin induces accumulation in tissue of innate immune cells associated with allergy. *Nature* **447**, 92–96 (2007).
26. R. Kuruvilla, L. S. Zweifel, N. O. Glebova, B. E. Lonze, G. Valdez, H. Ye, D. D. Ginty, A neurotrophin signaling cascade coordinates sympathetic neuron development through differential control of TrkA trafficking and retrograde signaling. *Cell* **118**, 243–255 (2004).
27. P. Sui, D. L. Wiesner, J. Xu, Y. Zhang, J. Lee, S. Van Dyken, A. Lashua, C. Yu, B. S. Klein, R. M. Locksley, G. Deutsch, X. Sun, Pulmonary neuroendocrine cells amplify allergic asthma responses. *Science* **360**, eaan8546 (2018).
28. K. S. Williams, D. A. Killebrew, G. P. Clary, J. A. Seawell, R. B. Meeker, Differential regulation of macrophage phenotype by mature and pro-nerve growth factor. *J. Neuroimmunol.* **285**, 76–93 (2015).
29. S. W. Brown, R. T. Meyers, K. M. Brennan, J. M. Rumble, N. Narasimhachari, E. F. Perozzi, J. J. Ryan, J. K. Stewart, K. Fischer-Stenger, Catecholamines in a macrophage cell line. *J. Neuroimmunol.* **135**, 47–55 (2003).
30. X. Ding, H. Wang, X. Qian, X. Han, L. Yang, Y. Cao, Q. Wang, J. Yang, Panicle-shaped sympathetic architecture in the spleen parenchyma modulates antibacterial innate immunity. *Cell Rep.* **27**, 3799–3807.e3 (2019).
31. Q. Wang, K. Liu, L. Yang, H. Wang, J. Yang, BoneClear: Whole-tissue immunolabeling of the intact mouse bones for 3D imaging of neural anatomy and pathology. *Cell Res.* **29**, 870–872 (2019).
32. L. J. Quinton, S. Nelson, P. Zhang, D. M. Boé, K. I. Happel, W. Pan, G. J. Bagby, Selective transport of cytokine-induced neutrophil chemoattractant from the lung to the blood facilitates pulmonary neutrophil recruitment. *Am. J. Physiol. Lung Cell. Mol. Physiol.* **286**, L465–L472 (2004).
33. E. Kolaczkowska, P. Kubes, Neutrophil recruitment and function in health and inflammation. *Nat. Rev. Immunol.* **13**, 159–175 (2013).
34. A. E. Price, H. E. Liang, B. M. Sullivan, R. L. Reinhardt, C. J. Eisley, D. J. Erle, R. M. Locksley, Systemically dispersed innate IL-13-expressing cells in type 2 immunity. *Proc. Natl. Acad. Sci. U.S.A.* **107**, 11489–11494 (2010).
35. H. Spits, D. Artis, M. Colonna, A. Diefenbach, J. P. Di Santo, G. Eberl, S. Koyasu, R. M. Locksley, A. N. McKenzie, R. E. Mebius, F. Powrie, E. Vivier, Innate lymphoid cells—A proposal for uniform nomenclature. *Nat. Rev. Immunol.* **13**, 145–149 (2013).
36. M. Ebbo, A. Crinier, F. Vely, E. Vivier, Innate lymphoid cells: Major players in inflammatory diseases. *Nat. Rev. Immunol.* **17**, 665–678 (2017).
37. F. Y. Liew, J. P. Girard, H. R. Turnquist, Interleukin-33 in health and disease. *Nat. Rev. Immunol.* **16**, 676–689 (2016).
38. M. Bosmann, J. J. Grailer, K. Zhu, M. A. Matthay, J. V. Sarma, F. S. Zetoune, P. A. Ward, Anti-inflammatory effects of β2 adrenergic receptor agonists in experimental acute lung injury. *FASEB J.* **26**, 2137–2144 (2012).
39. S. Moriyama, J. R. Brestoff, A. L. Flamar, J. B. Moeller, C. S. N. Klose, L. C. Rankin, N. A. Yudanin, L. A. Monticelli, G. G. Putzel, H. R. Rodewald, D. Artis, β2-adrenergic receptor-mediated negative regulation of group 2 innate lymphoid cell responses. *Science* **359**, 1056–1061 (2018).
40. B. N. Lambrecht, H. Hammad, The immunology of asthma. *Nat. Immunol.* **16**, 45–56 (2015).
41. P. J. Barnes, Targeting cytokines to treat asthma and chronic obstructive pulmonary disease. *Nat. Rev. Immunol.* **18**, 454–466 (2018).
42. A. Papi, C. Brightling, S. E. Pedersen, H. K. Reddel, Asthma. *Lancet* **391**, 783–800 (2018).
43. G. Matute-Bello, G. Downey, B. B. Moore, S. D. Groshong, M. A. Matthay, A. S. Slutsky, W. M. Kuebler, G. Acute, An official American Thoracic Society workshop report: Features and measurements of experimental acute lung injury in animals. *Am. J. Respir. Cell Mol. Biol.* **44**, 725–738 (2011).
44. A. E. Kelly-Welch, M. E. Melo, E. Smith, A. Q. Ford, C. Haudenschild, N. Noben-Trauth, A. D. Keegan, Complex role of the IL-4 receptor alpha in a murine model of airway inflammation: Expression of the IL-4 receptor alpha on nonlymphoid cells of bone marrow origin contributes to severity of inflammation. *J. Immunol.* **172**, 4545–4555 (2004).

Acknowledgments

Funding: This work was supported by the National Key Research and Development Program of China (2019YFA0802003) and the National Natural Science Foundation of China (to J.Y.; #31522024, #31771111, and #31970974). Additional supports were provided by the Center for Life Sciences, the School of Life Sciences, the IDG/McGovern Institute for Brain Research, and the State Key Laboratory of Membrane Biology at Peking University, and by the Institute of Molecular Physiology at the Shenzhen Bay Laboratory. **Author contributions:** J.Y. conceived and designed the project as the senior and corresponding author. T.L., L.Y., X.H., and X.D. performed the experiments and analyzed the results under J.Y.'s supervision. J.L. helped collect the macaque lung tissues. **Competing interests:** The authors declare that they have no competing interests. **Data and materials availability:** All data needed to evaluate the conclusions in the paper are present in the paper and/or the Supplementary Materials. Additional data related to this paper may be requested from the authors. Further information and requests for resources or reagents should be directed to and will be fulfilled by the corresponding author J.Y. (jing.yang@pku.edu.cn).

Submitted 11 June 2019
Accepted 28 February 2020
Published 13 May 2020
10.1126/sciadv.aay1497

Citation: T. Liu, L. Yang, X. Han, X. Ding, J. Li, J. Yang, Local sympathetic innervations modulate the lung innate immune responses. *Sci. Adv.* **6**, eaay1497 (2020).

Science Advances

Local sympathetic innervations modulate the lung innate immune responses

Tingting Liu, Lu Yang, Xiangli Han, Xiaofan Ding, Jiali Li and Jing Yang

Sci Adv **6** (20), eaay1497.
DOI: 10.1126/sciadv.aay1497

Science Advances (ISSN 2375-2548) is published by the American Association for the Advancement of Science, 1200 New York Avenue NW, Washington, DC 20005. The title *Science Advances* is a registered trademark of AAAS.